SAND2022-13170C

Noncontinuum Effects at the Smallest Scales of Turbulence

M. A. Gallis[a], R. M. McMullen[b], M. C. Krygier[c], J. R. Torczynski[d]

Engineering Sciences Center, Sandia National Laboratories,
P. O. Box 5800, Albuquerque, New Mexico 87185-0840 USA
[a]Corresponding author: magalli@sandia.gov
[b]rmmcmul@sandia.gov, [c]mkrygie@sandia.gov, [d]jrtorcz@sandia.gov

Abstract. Currently accepted turbulence theory assumes that the flow is continuum at all length scales, including the smallest length scale of turbulence, known as the Kolmogorov scale. Kolmogorov in his celebrated 1941 theory [A. N. Kolmogorov, C. R. Acad. Sci. URSS 30, 301-305 (1941)] asserted that the fine-scale turbulent structures in the energy cascade are universal. According to Kolmogorov's theory, the energy dissipation rate and kinematic viscosity alone describe this universal behavior in terms of the Kolmogorov length, time, and velocity scales. However, it has been suggested [R. Betchov, J. Fluid Mech. 3, 205-216 (1957); D. Bandak, N. Goldenfeld, A. A. Mailybaev, and G. Eyink, Phys. Rev. E 105, 065113 (2022)] that thermal fluctuations, absent from the continuum description of gases, can terminate the energy cascade at a length scale larger than mean-free-path considerations alone would suggest. Additionally, for high-Mach-number turbulent flows, the Kolmogorov length scale can be comparable to the gas-molecule mean free path, which could induce noncontinuum molecular-level effects in the turbulent energy cascade. To investigate these two issues, compressible Taylor-Green vortex flow is simulated using the direct simulation Monte Carlo (DSMC) method and direct numerical simulations (DNS) of the Navier-Stokes equations. It is found that the molecular-gas-dynamics spectra grow quadratically with wavenumber in the dissipation range due to thermal fluctuations instead of decreasing exponentially as the continuum description predicts. Macroscopically, thermal fluctuations appear to break the flow symmetries and thereby produce different but statistically similar routes from the initial non-turbulent flow to the long-time turbulent flow.

Turbulent flows are composed of eddies with a wide range of sizes. Turbulent kinetic energy cascades down from large-scale eddies to smaller-scale eddies until a scale is reached at which viscous dissipation becomes significant [1]. Dimensional arguments, which have traditionally been employed to estimate the range of scales, have led to the conclusion that the smallest length scales are much larger than the mean free path [2,3]. Therefore, the continuum approximation is considered to be valid, so the Navier-Stokes (NS) equations should in principle be capable of accurately reproducing all length scales, including the smallest length scales of turbulence. This assertion has been supported by the success of the NS equations in reproducing numerous experimental observations although the smallest scales of turbulence have never been experimentally observed. However, this assertion may need to be reassessed for the smallest flow-field features in the light of some early and recent investigations.

Betchov in 1957 [4] and Bandak et al. in 2022 [5] suggested that thermal fluctuations, absent from the continuum description of gases, can impact the energy cascade at a length scale larger than mean-free-path considerations alone would suggest. More specifically, noncontinuum molecular-level effects modify the turbulent energy spectrum near the Kolmogorov length scale even though the gas-molecule mean free path is much smaller. Numerical simulations have confirmed these findings not only for gases, as in McMullen et al. [6], but also for liquids, as in Bell et al. [7].

Understanding the behavior of turbulent flow at dissipation-range length scales, including the dominant processes of energy transfer in this regime, is not simply an academic problem [8]. In numerical analyses, the smallest length scales in such flows constrain the size of the numerical mesh. Similarly, in experimental work, the smallest length and velocity scales in such flows constrain the sensing volume of a probe and its required velocity resolution.

The purpose of this work is to investigate the behavior of the smallest scales of turbulence beyond the point reached by any experimental technique to date. To this end, three-dimensional decaying turbulent flows are simulated using two completely different techniques: the molecular-level Direct Simulation Monte Carlo (DSMC) method of Bird [9] and a continuum-level Direct Numerical Simulation (DNS) solver of the NS equations [10].

DSMC [9] was developed over 50 years ago by Graeme A. Bird and is now a well-established molecular-level technique for modeling low-density gas flows. Recent advances in supercomputing technology (currently at the exascale level) have now brought higher-density near-continuum flows within reach [6,11-18]. At these high densities, the Reynolds numbers can become large enough for the flows to be in the turbulent regime.

By way of contrast, DNS assumes that the flows to be simulated are continuum (or perhaps near-continuum with slip-jump boundary conditions). Molecular-level phenomena such as thermal fluctuations, which are absent from the NS equations, are not usually considered. Thus, DNS attempts to reproduce all length and time scales in the flow.

Herein, the effects of thermal fluctuations on the turbulent energy cascade are studied. This investigation is carried out by performing DSMC molecular-level simulations and DNS continuum simulations of Taylor-Green vortex flow, a canonical turbulent flow studied extensively by many investigators, and comparing these results.

TAYLOR-GREEN VORTEX FLOW WITH ISOTHERMAL INITIAL CONDITIONS

The turbulent flow examined herein is Taylor-Green (TG) vortex flow [19,20]. TG flow is a canonical turbulent flow in which the generation of small-scale eddies and the corresponding cascade of energy from small to large wavenumbers can be observed numerically. TG flow is initialized in a triply periodic domain $-\pi L \le \{x,y,z\} \le \pi L$ using velocity and pressure fields having only a single length scale L and a single velocity scale V_0:

$$\begin{aligned} u &= V_0 \sin(x/L)\cos(y/L)\cos(z/L) \\ v &= -V_0 \cos(x/L)\sin(y/L)\cos(z/L) \\ w &= 0 \\ p &= p_0 + (\rho_0 V_0^2/16)(\cos(2x/L)+\cos(2y/L))(\cos(2z/L)+2) \\ \rho &= mp/k_B T_0 \\ T &= T_0. \end{aligned} \tag{1}$$

Here, $\mathbf{u} = (u,v,w)$, p, ρ, and T are the velocity, pressure, density, and temperature at position $\mathbf{x} = (x,y,z)$ and nondimensional time $\tilde{t} = 0$, where $\tilde{t} = V_0 t/L$. Thus, all the kinetic energy is initially resident in a single wavenumber. The gas has molecular mass m, specific heat ratio γ, and viscosity μ, which is a function of the temperature T. The Boltzmann constant is k_B. The gas obeys the ideal gas law $\rho = mp/k_B T$ and has sound speed $a = \sqrt{\gamma k_B T/m}$, most probable molecular speed $c = \sqrt{8k_B T/\pi m}$, and mean free path $\lambda = 2\mu/\rho c$. Reference values are denoted by the subscript "0". Together, these quantities yield three nondimensional quantities (only two are independent): Mach number $\mathrm{Ma} = V_0/a_0$, Reynolds number $\mathrm{Re} = \rho_0 V_0 L/\mu_0$, and Knudsen number $\mathrm{Kn} = \lambda/L = \sqrt{\pi\gamma/2}\,\mathrm{Ma}/\mathrm{Re}$.

The DSMC code SPARTA [11,16] is used to simulate TG flow. SPARTA is an exascale-class open-source code capable of running efficiently on massively parallel, heterogeneous-architecture computational platforms. The computational domain is the cube defined by $-\pi L \le \{x,y,z\} \le \pi L$, where the domain length scale is $L = 0.0001$ m. The domain is divided into 8 billion cells (2000^3) with 45 particles/cell on average for a total of 0.36 trillion particles. The gas has argon properties: molecular mass $m = 66.3\times10^{-27}$ kg and specific heat ratio $\gamma = 5/3$, with reference values $p_0 = 88414.7$ Pa, $T_0 = 273.15$ K, and $\rho_0 = 1.5544$ kg/m^3, which yield a sound speed of $a_0 = 307.9$ m/s.

Four values of the Mach number are simulated: $\mathrm{Ma} = 0.3,\ 0.6,\ 0.9,\ 1.2$. Since the initial temperature is the same, the velocity V_0 is directly proportional to the Mach number. The case with $\mathrm{Ma} = 0.3$ is nearly incompressible, but, as the Mach number is increased, the cases become progressively more compressible. At long times, the temperature is increased above the initial value due to thermalizing the initial kinetic energy. This temperature increase is slightly over 1% for the $\mathrm{Ma} = 0.3$ case and about 20% for the $\mathrm{Ma} = 1.2$ case.

Molecular collisions are performed using the Variable Soft Sphere (VSS) model [9]. To improve spatial discretization, collision partners are selected from within a sphere having a radius that equals the distance traveled by the particle during the time step [11]. Multiple collisions between the same two molecules during the same time step are not allowed. Based on DSMC simulations of two-dimensional TG flow, this procedure yields a viscosity that is only 36% higher than the nominal value for argon even though the cell size is rather large: $\Delta s = 3.24\lambda$. However, the Reynolds number is based on the simulation viscosity rather than the nominal argon value, which yields the following four values of the Reynolds number: $\mathrm{Re} = 500,\ 1000,\ 1500,\ 2000$. These Reynolds and Mach numbers correspond to a single value of the Knudsen number for all four cases: $\mathrm{Kn} = 0.00097$.

The Sandia Parallel Aerodynamics and Reentry Code SPARC [10] is also used to simulate TG flow. SPARC uses a shock-capturing finite-volume method to achieve stability in the presence of strong shock waves and high accuracy in smooth regions of the flow. This is achieved by blending two numerical methods. The first is the modified Steger-Warming method [21], which offers good numerical stability but generates appreciable numerical dissipation. The second is the kinetic-energy-consistent central-difference scheme of Subbareddy and Candler [22], which produces high-order spatial accuracy and lower numerical dissipation at the expense of reduced numerical stability. The method switches between these two schemes using gradients in the Mach number to detect shocks and apply the stabilizing modified Steger-Warming fluxes in those regions. The result is an overall scheme that has good accuracy in smooth parts of the flow and is robust to shock waves. Time advancement is accomplished using a third-order explicit Runge-Kutta method with a Courant-Friedrichs-Lewy number of 0.5 to determine the time step.

SPARC DNS results on 512^3 and 1024^3 meshes are compared. The corresponding dissipation rates are almost indistinguishable for $\mathrm{Ma} = 0.3\text{-}0.9$, and only slight differences are observed for $\mathrm{Ma} = 1.2$. Thus, the SPARC results on the 512^3 mesh are deemed to be sufficiently converged for the purposes herein.

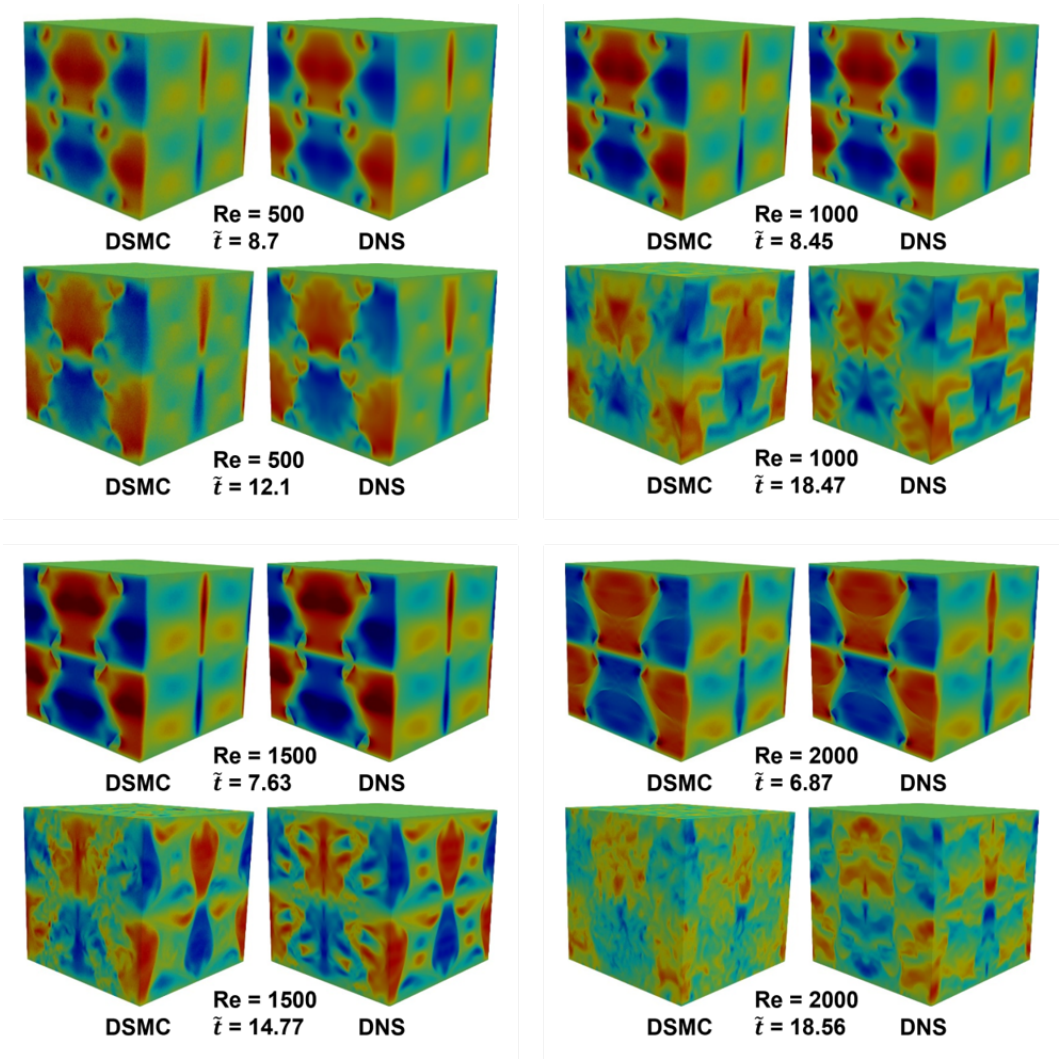

Figure 1. Vertical velocity component for all four Reynolds numbers.

Figure 1 presents the vertical velocity component on the bounding planes of the domain from the DSMC and DNS simulations at times before and after the times of maximum dissipation, which occurs around $\tilde{t} = 9$ for all four cases. To reduce statistical scatter, the DSMC results are averaged over an interval of 10,000 time steps, which corresponds to 5% of the Kolmogorov time scale $\tau_\eta = \left(\langle \nu \rangle / \langle \varepsilon \rangle\right)^{1/2}$.

Before the maximum-dissipation time, except for being slightly noisier, the DSMC results are virtually identical to the DNS results for all four cases. Large-scale structures, which are remnants of the initial conditions, are clearly discernible, and smaller-scale structures appear and grow. Up to the time of maximum dissipation, the DSMC and DNS flow fields both preserve the initial symmetries of both large-scale and small-scale features. After the maximum dissipation time, the DSMC and DNS flow fields begin to exhibit differences. More specifically, the DNS flow fields continue to preserve the symmetries of the initial conditions, but the DSMC flow fields no longer do so. These differences are small for the lowest Mach and Reynolds numbers but become more significant with increasing Mach and Reynolds numbers. These differences possibly arise from the small-scale disturbances caused by thermal fluctuations, which then gradually propagate up to the large scales, though the precise mechanism by which this happens is not currently understood.

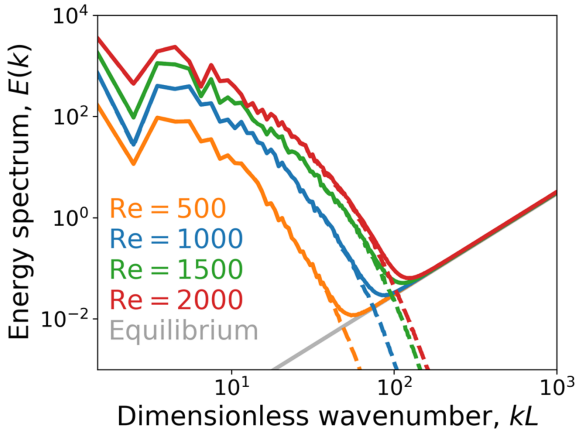

Figure 2. DSMC (solid curves) and DNS (dashed curves) kinetic-energy spectra for all four Reynolds numbers.

Figure 2 presents DSMC and DNS three-dimensional kinetic-energy spectra near the maximum dissipation time. The DSMC spectra are computed from instantaneous flow fields (no time averaging is performed). Thermal fluctuations and their overlap with the small length scales of turbulence are seen in the DSMC spectra at large wavenumbers k (i.e., at small wavelengths). As time progresses, the kinetic energy in the low-wavenumber (large-wavelength) region of the spectrum is transferred from the initial low wavenumber to the larger wavenumbers (i.e., from larger wavelengths to smaller wavelengths). The DSMC and DNS spectra agree very well for wavelengths less than roughly the Kolmogorov length scale $\eta = \left(\langle \nu \rangle^3 / \langle \varepsilon \rangle\right)^{1/4}$, where $\nu = \mu/\rho$ and $\langle \varepsilon \rangle$ is the mean energy dissipation rate. For $k > k_c$, the crossover wavenumber, the DNS spectra decay exponentially fast, but the DSMC spectra become proportional to k^2. This quadratic dependence is the signature of thermal noise due to molecular fluctuations. In these DSMC simulations, the equilibrium portion of the spectrum is overestimated because the simulation ratio is $F > 1$. However, the correct equilibrium spectrum can be obtained by extrapolating to a simulation ratio of unity [6]. Doing so yields the crossover wavenumber $k_c \eta \approx 3$ [6]. As Bandak et al. [5] point out, the presence of a new parameter $k_B T$ invalidates Kolmogorov's postulate that the only relevant parameters are the kinematic viscosity and mean energy dissipation rate [1].

We emphasize that it was traditionally believed that thermal fluctuations are important only when the characteristic flow length scale (here, η) approaches the order of the mean molecular spacing $\delta = \left(m/\rho\right)^{1/3}$ [9]. However, Figure 2 indicates that this assumption is not true when applied to the dissipation range of the energy spectrum. Indeed, at $\tilde{t} = 9$ this ratio is $\eta/\delta = 323$ for the case with $\mathrm{Ma} = 1.2$ and $\mathrm{Re} = 2000$ and $\eta/\delta = 836$ for the case with $\mathrm{Ma} = 0.3$ and $\mathrm{Re} = 500$. Consequently, thermal fluctuations are significant at scales much larger than previously believed.

In summary, molecular fluctuations dominate the dissipation range and are potentially responsible for differences in the realization for the large scales as compared to DNS, which lacks thermal fluctuations. The large-scale differences are accentuated as the Mach and Reynolds numbers are increased. The mechanism through which this occurs is not currently understood and should be the subject of future work. However, we note that, although the domain-scale Knudsen number $\mathrm{Kn} = \lambda/L$ is the same for all four cases considered herein, the Knudsen number based on the Kolmogorov scale $\mathrm{Kn}_\eta = \lambda/\eta$ increases with increasing Reynolds number, implying that noncontinuum effects within the dissipation range become more pronounced.

TAYLOR-GREEN VORTEX FLOW WITH POLYTROPIC INITIAL CONDITIONS

To further investigate compressibility effects, DSMC and DNS simulations of compressible Taylor-Green (TG) vortex flow are performed using polytropic initial conditions. Polytropic initial conditions allow higher Mach numbers (up to $\mathrm{Ma} = 2$ for a specific heat ratio $\gamma = 5/3$) than are possible using only a constant-temperature initial condition. As above, SPARTA is used to perform the DSMC simulations, and SPARC is used to perform the DNS simulations. The velocity fields and kinetic-energy spectra from these simulations at selected times are then compared.

As in the previous section, TG flow is initialized in a triply periodic domain $-\pi L \le \{x, y, z\} \le \pi L$ using velocity and pressure fields having only a single length scale L and a single velocity scale V_0:

$$
\begin{aligned}
u &= V_0 \sin(x/L)\cos(y/L)\cos(z/L) \\
v &= -V_0 \cos(x/L)\sin(y/L)\cos(z/L) \\
w &= 0 \\
\frac{T}{T_0} &= 1 + (\gamma - 1)\frac{\mathrm{Ma}^2}{16}\left(\cos(2x/L) + \cos(2y/L)\right)\left(\cos(2z/L) + 2\right) \\
\frac{\rho}{\rho_0} &= \left(\frac{T}{T_0}\right)^{1/(\gamma-1)} \\
\frac{p}{p_0} &= \left(\frac{\rho}{\rho_0}\right)^{\gamma}.
\end{aligned}
\tag{2}
$$

However, in the above, the initial temperature is not constant. Instead, the initial distributions of temperature, density, and pressure are related in an adiabatic fashion using the specific heat ratio γ.

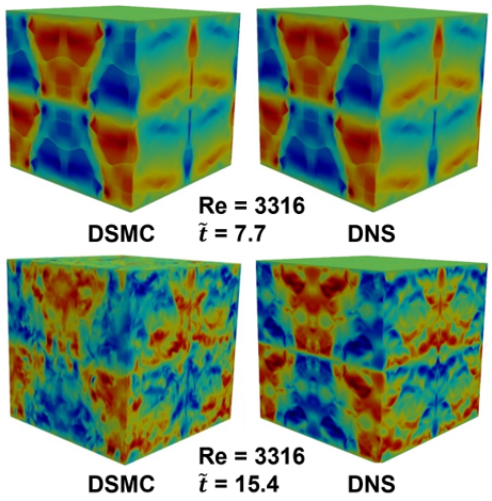

Figure 3. Vertical velocity component for $\mathrm{Re} = 3316$ with polytropic initial conditions.

Figure 3 presents the vertical velocity component on the bounding planes of the domain from the DSMC and DNS simulations at times before and after the time of maximum dissipation, which again occurs near $\tilde{t} = 9$ for this case. To reduce statistical scatter, the DSMC results are averaged over 10,000 time steps, which is a small fraction of the Kolmogorov time scale. The results are basically similar to the $\mathrm{Ma} = 1.2$ case presented in the previous section. Before the maximum dissipation time, except for being noisier, the DSMC and DNS results are virtually identical. After the maximum dissipation time, the DSMC and DNS results exhibit the differences noted in the previous section: the DNS results continue to preserve the symmetries of the initial conditions, but the DSMC results do not.

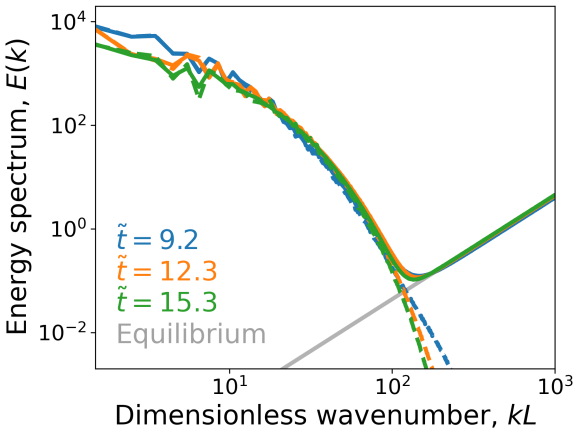

Figure 4. DSMC (solid curves) and DNS (dashed curves) kinetic-energy spectra at three different times for $\mathrm{Re} = 3316$ with polytropic initial conditions.

Figure 4 presents DSMC and DNS three-dimensional kinetic-energy spectra (the distribution of kinetic energy as a function of wavenumber k) at three times. As in Figure 2, the DSMC spectra shown in Figure 4 are computed from instantaneous flow fields (no time averaging is performed). These spectra exhibit the same behavior as the spectra in Figure 2. The DSMC and DNS spectra agree very well for large scales, corresponding to wavelengths well greater than roughly the Kolmogorov length scale η. For small wavelengths ($k\eta > 1$), the NS spectrum decays exponentially fast, but the DSMC spectrum grows proportional to k^2. Therefore, for the ranges of Reynolds and Mach numbers considered herein, no significant departures from local thermodynamic equilibrium are observed.

MODEL ACCOUNTING FOR THERMAL-FLUCTUATION EFFECTS ON STATISTICS

The fact that the energy spectrum in DSMC exhibits scaling consistent with equilibrium thermal fluctuations for $k > k_c$ motivates a superposition model for the small-scale statistics of the velocity field. Essentially, we add a thermal-fluctuation velocity component to the Navier-Stokes (NS) velocity field:

$$u_i = u_i^{\mathrm{NS}} + u_i^{\mathrm{th}}, \tag{3}$$

where the thermal-fluctuation component u_i^{th} is Maxwellian, i.e.,

$$u_i^{\mathrm{th}} \sim \mathcal{N}\left(0, Fk_B T_0 / \rho l^3\right), \tag{4}$$

and l^3 is an averaging (or coarse-graining) volume centered at the point $\mathbf{x}$. Consequently, this model is strictly valid only at scales larger than l. In the DSMC simulations, l^3 is simply the cell volume. We note that the assumption of equilibrium fluctuations is similar to that made in fluctuating hydrodynamics [5,7], in which includes stochastic fluxes with Gaussian white noise statistics in the NS equations. The model thus implicitly assumes local thermodynamic equilibrium and, therefore, cannot be applied when nonequilibrium effects are significant. However, none of the cases considered herein exhibit strong nonequilibrium effects.

It is further assumed that the thermal-fluctuation and NS components are statistically independent, such that

$$\left\langle \left(u_i^{\mathrm{NS}}\right)^m \left(u_i^{\mathrm{th}}\right)^n \right\rangle = \left\langle \left(u_i^{\mathrm{NS}}\right)^m \right\rangle \left\langle \left(u_i^{\mathrm{th}}\right)^n \right\rangle \tag{5}$$

for any moment orders m, n. This implies that the energy spectrum may be written as

$$E(k) = E^{\mathrm{NS}}(k) + E^{\mathrm{th}}(k). \tag{6}$$

This expression is plotted in Figure 5 along with the DSMC spectrum for the $\mathrm{Re} = 500$, $\mathrm{Ma} = 0.3$ case at $\tilde{t} = 9$ near the crossover wavenumber k_c, which demonstrates excellent agreement between the two. However, we note that the k^2 portion of the DSMC spectrum in Figure 5 sits very slightly (~3%) above the theoretical prediction for the

equilibrium spectrum. A small part of this discrepancy can be accounted for by the slight temperature rise by $\tilde{t} = 9$. A possible explanation for the remainder of the discrepancy is that using an average of 45 simulators per cell slightly under-samples the velocity distribution function, resulting in a small bias. This explanation is supported by the fact that simulations of an equilibrium gas with larger numbers of simulators per cell causes this discrepancy to disappear. Nonetheless, this can be accounted for through an effective simulation ratio $F' \approx 1.03F$; we use this value in the subsequent comparison of the model with the DSMC simulations.

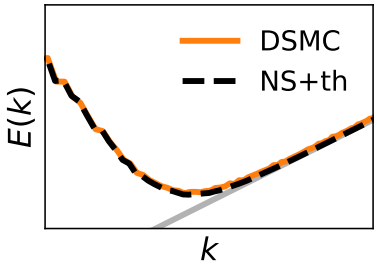

Figure 5. Energy spectrum in the vicinity of the crossover wavenumber k_c for the $\mathrm{Re} = 500$, $\mathrm{Ma} = 0.3$ case from Figure 2 at $\tilde{t} = 9$. The gray line represents the theoretical prediction for the equilibrium spectrum.

Next, we use this model to make predictions about other statistics. In particular, we focus on the longitudinal velocity structure functions, which are commonly used to quantify intermittency effects [23,24]. The n^{th}-order longitudinal structure function is the n^{th} moment of the longitudinal velocity increment between points $\mathbf{x}$ and $\mathbf{x}+\mathbf{r}$:

$$\begin{aligned} S_n(r) &= \langle (\delta u_r^L)^n \rangle, \\ \delta u_r^L &= u(x+r) - u(x), \\ u &= \mathbf{u}\cdot\mathbf{r}/r, \\ x &= \mathbf{x}\cdot\mathbf{r}/r, \end{aligned} \tag{7}$$

where $r = |\mathbf{r}|$ is the separation magnitude. Substituting eqs. (3) and (4) and utilizing eq. (5) yields

$$\begin{aligned} S_n(r) &= \langle (\delta_r u^{\mathrm{NS}} + \delta_r u^{\mathrm{th}})^n \rangle \\ &= \sum_{k=0}^{n} \binom{n}{k} \left\langle \left(\delta_r u^{\mathrm{NS}}\right)^{n-k} \left(\delta_r u^{\mathrm{th}}\right)^k \right\rangle \\ &= \sum_{k=0}^{n} \binom{n}{k} S_{n-k}^{\mathrm{NS}}(r) \left\langle \left(\delta_r u^{\mathrm{th}}\right)^k \right\rangle \\ &= S_n^{\mathrm{NS}}(r) + \sum_{p=1}^{\lfloor n/2 \rfloor} \binom{n}{2p} 2^p (2p-1)!! \left(\frac{F k_B T_0}{\rho l^3}\right)^p S_{n-2p}^{\mathrm{NS}}(r), \end{aligned} \tag{8}$$

where $\lfloor\ \rfloor$ denotes rounding toward 0. Since we herein are concerned primarily with small scales, we nondimensionalize $S_n(r)$ using the Kolmogorov velocity u_η, giving

$$\frac{S_n(r)}{u_\eta^n} = \frac{S_n^{\mathrm{NS}}(r)}{u_\eta^n} + \sum_{p=1}^{\lfloor n/2 \rfloor} \binom{n}{2p} 2^p (2p-1)!! F^p \Theta_\eta^p \left(\frac{l}{\eta}\right)^{-3p} \frac{S_{n-2p}^{\mathrm{NS}}(r)}{u_\eta^{n-2p}}, \tag{9}$$

where we have introduced the dimensionless temperature [5]

$$\Theta_\eta = \frac{k_B T_0}{\rho u_\eta^2 \eta^3}. \tag{10}$$

The first term on the right-hand-side of eq. (9) is the NS contribution to $S_n(r)$, and the summation term represents the contribution of thermal fluctuations. Note that this term is a weighted sum of lower-order NS structure functions, and, therefore, that the thermal-fluctuation contribution is possibly felt even at large r. However, the parameter Θ_η is

typically quite small ($\sim 10^{-9} - 10^{-6}$) [5-7]. Furthermore, the appearance of the simulation ratio F in eq. (9) means that the thermal-fluctuation contribution to the structure functions is overestimated in the DSMC simulations, as discussed in McMullen et al. [6].

In analogy with the crossover wavenumber k_c, we can define a crossover separation r_c below which thermal fluctuations can be expected to dominate. An order-of-magnitude estimate for r_c may be obtained from eq. (9) as follows. First, we utilize an approximation of $S_n^{\mathrm{NS}}(r)$, which becomes valid as $r \to 0$. In this limit, it is assumed that $\mathbf{u}^{\mathrm{NS}}$ is analytic, such that, to leading order,

$$\frac{S_n^{\mathrm{NS}}(r)}{u_\eta^n} \approx A_n \left(\frac{r}{\eta}\right)^n, \tag{11}$$

where $A_n = \langle (\partial_x u)^n \rangle$ [24]. Therefore, in the so-called analytic range,

$$\frac{S_n(r)}{u_\eta^n (r/\eta)^n} = A_n + \sum_{p=1}^{\lfloor n/2 \rfloor} \binom{n}{2p} 2^p (2p-1)!! F^p \Theta_\eta^p \left(\frac{l}{\eta}\right)^{-3p} A_{n-2p} \left(\frac{r}{\eta}\right)^{-2p}. \tag{12}$$

Conservatively, the contributions of the thermal-fluctuation term is thus the same order of magnitude as the NS term when

$$A_n \sim n(n-1) F \Theta_\eta \left(\frac{l}{\eta}\right)^{-3} A_{n-2} \left(\frac{r_c}{\eta}\right)^{-2}, \tag{13}$$

whence

$$\frac{r_c}{\eta} \sim \left(n(n-1) \frac{A_{n-2}}{A_n} F \Theta_\eta \right)^{1/2} \left(\frac{l}{\eta}\right)^{-3/2}. \tag{14}$$

The dependence of r_c on the ratio l/η reflects the intuition that, for fixed η, attempting to resolve smaller and smaller scales, i.e., decreasing the size of the coarse-graining volume l^3, will result in more pronounced effects of thermal fluctuations. We note that a more refined estimate may be possible with further assumptions on the behavior of the velocity gradient moments A_n with both moment order *n* and Reynolds number Re. However, this is beyond the scope of the present paper and will be left for future work. Finally, since the thermal-fluctuation model, eqs. (3) and (4), is valid only for $r > l$, eq. (14) may be inverted to give a necessary condition for thermal fluctuation effects to be observable in the structure functions:

$$\frac{l}{\eta} < \left(n(n-1) \frac{A_{n-2}}{A_n} F \Theta_\eta \right)^{1/5}. \tag{15}$$

Next, we test the model predictions against structure functions computed directly from the DSMC simulations. Here, we focus on the low-order moments $n = 2\text{-}4$. For concreteness, the explicit expressions for these structure functions, obtained from eq. (8), are provided here:

$$\begin{aligned} S_2(r) &= S_2^{\mathrm{NS}}(r) + 2\frac{F k_B T_0}{\rho l^3}, \\ S_3(r) &= S_3^{\mathrm{NS}}(r), \\ S_4(r) &= S_4^{\mathrm{NS}}(r) + 12\frac{F k_B T_0}{\rho l^3} S_2^{\mathrm{NS}}(r) + 12\left(\frac{F k_B T_0}{\rho l^3}\right)^2. \end{aligned} \tag{16}$$

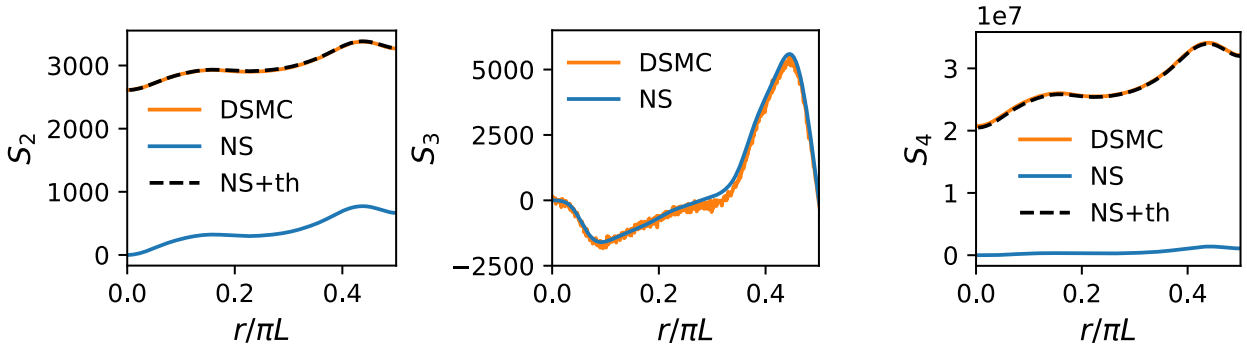

Figure 6. Comparison of structure functions for $n = 2\text{-}4$ predicted by the fluctuation model, eq. (16) with those computed directly from DSMC for $\mathrm{Re} = 500,\ \mathrm{Ma} = 0.3$.

The results of the comparison for the $\mathrm{Re} = 500,\ \mathrm{Ma} = 0.3$ case are shown in Figure 6, which demonstrates that the prediction given by the model in eq. (16) is quite good. Also shown are the NS structure functions. For S_3, the NS and DSMC structure functions agree very well since, according to eq. (16), thermal fluctuations make no contribution. On the other hand, the difference between NS and DSMC is large across the entire domain for S_2 and S_4. For S_2, this amounts to only a vertical shift. However, the shape of S_4 is modified in addition to a shift due to the second term, which is proportional to S_2^{NS}. As discussed above, these thermal-fluctuation contributions are magnified due to the use of a simulation ratio $F > 1$. Nonetheless, Figures 5 and 6 demonstrate the validity of this fluctuation model.

Now that the predictions of the model have been validated against DSMC, we set $F = 1$ in eq. (16) in order to estimate the separation r_c below which thermal-fluctuation effects would be observable in a real gas. The results are shown in Figure 7, which indicates that thermal-fluctuation corrections to the structure functions become significant for $r < \eta$, consistent with observations that $k_c\eta \approx 3$ [6,7]. The right panel of Figure 7 plots the relative magnitude of the thermal-fluctuation and NS contributions, which shows that the thermal fluctuation term is $\sim 5\%$ for $r \sim \eta$, but that it grows like r^{-2} as $r \to l$.

Several conclusions can be drawn from these results. First, is that the analytic range in which eq. (11) is valid must be limited to $l << r << \eta$; as $r \to l$, the (even-order) structure functions tend to a constant value. Second, the long-range nature of the thermal-fluctuation terms in eq. (9) means that they could potentially affect the structure functions at scales significantly larger than η. However, any such modification will likely be quite small owing to the smallness of Θ_η. Nonetheless, this may have implications for intermittency models [23,24].

Finally, we note that the model presented in this section should be viewed as a statistical model, as opposed to a dynamical one (like fluctuating hydrodynamics [5,7]). That is, it cannot be expected to accurately reproduce the evolution of a flow with thermal fluctuations. This is apparent if one considers Figures 1 and 3: Adding a thermal-fluctuation velocity to the DNS fields would result in only small-scale noise and could not account for the large-scale fluctuations observed in the DSMC fields.

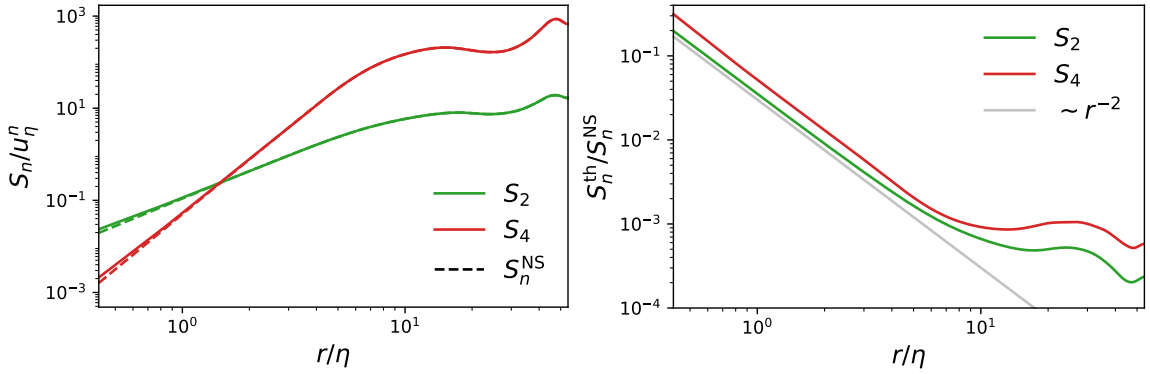

Figure 7. (Left) Predictions for thermal fluctuation effects on structure functions S_2 and S_4 for $\mathrm{Re} = 500,\ \mathrm{Ma} = 0.3$ with $F = 1$; the solid and dashed lines are eq. (16) and the NS structure functions, respectively. (Right) The relative magnitude of the thermal-fluctuation and NS terms in eq. (16).

DISCUSSION AND CONCLUSIONS

The present work extends the work of McMullen et al. [6] by considering higher Mach and Reynolds numbers and polytropic initial conditions. These new results are qualitatively the same: the smallest scales in turbulent flows are dominated by thermal fluctuations, in contrast to the exponential decay predicted by the Navier-Stokes equations. Even at these higher Mach numbers, the kinetic-energy spectrum in the dissipation range remains proportional to k^2, suggesting no significant departures from local thermodynamic equilibrium.

Next, a superposition model was proposed to account for thermal-fluctuation effects on various statistics. The model assumes that the velocity field is the sum of the Navier-Stokes velocity and a statistically independent thermal-fluctuation velocity component having an equilibrium distribution. By comparison with statistics computed from the DSMC simulations, the model was shown to accurately account for the thermal-fluctuation modification of the energy spectrum and several low-order longitudinal velocity structure functions. An estimate for the separation r_c below which thermal fluctuations can be expected to significantly modify the structure functions was provided, and it was shown that, for the flow configurations considered herein, $r_c \sim \eta$, which is in agreement with the energy spectrum crossover length scale [6,7].

Despite the fact that thermal fluctuations were not observed herein to have a significant effect on the statistics of the large scales, Figures 1 and 3 provide strong evidence that thermal fluctuations influence their particular realization. It is thus natural to ask what the implications of unavoidable thermal fluctuations are for the predictability of turbulence. Even in the absence of thermal fluctuations, this is a subject of ongoing debate: Chaos theory states that two solutions separate exponentially fast [25-28], while other recent work has provided evidence that the separation rate is faster-than-exponential [29]. Yet other work argues that turbulent flows exhibit spontaneous stochasticity and are, therefore, fundamentally indistinguishable from random processes [30-33].

Interestingly, it has recently been shown that the small numerical noise introduced by truncation and roundoff errors in finite-precision arithmetic can be amplified sufficiently to influence large-scale features in simulations of deterministic turbulent flows and can even cause the flow to visit different attractors in state space, thereby altering the statistics [34]. It thus seems plausible that thermal fluctuations could result in similar behavior.

Additionally, the possibility of transition to turbulence due to thermal fluctuations has been investigated in the context of boundary-layer receptivity by Fedorov and Tumin [35] and Luchini [36]. They note that this implies an upper bound on the transition Reynolds number and conclude that, for hypersonic flight, thermal fluctuations may yield disturbances large enough to cause transition to turbulence. Further investigations of the influence of thermal fluctuations on hydrodynamic instabilities and transition to turbulence is thus another promising area of future work.

Ultimately, the fundamental question is whether the hydrodynamic equations can remain valid or whether the interaction of thermal fluctuations with the thermodynamic fluctuations can lead to a breakdown in the hydrodynamic description. Although a complete breakdown of the continuum description is not observed in the cases examined, the evidence herein suggests that the presence of thermal fluctuations can qualitatively change the flow. DSMC can complement DNS because phenomena such as thermal relaxation and chemical reactions can be incorporated into DSMC at the molecular level in a straightforward manner. As supercomputing technology continues to advance, even larger Reynolds numbers will come within reach of DSMC.

ACKNOWLEDGMENTS

Sandia National Laboratories is a multimission laboratory managed and operated by National Technology and Engineering Solutions of Sandia, LLC, a wholly owned subsidiary of Honeywell International, Inc., for the U.S. Department of Energy's National Nuclear Security Administration under contract DE-NA0003525. This paper describes objective technical results and analysis. Any subjective views or opinions that might be expressed in the paper do not necessarily represent the views of the U.S. Department of Energy or the United States Government. This manuscript has been authored by National Technology and Engineering Solutions of Sandia, LLC, under Contract No. DE-NA0003525 with the U.S. Department of Energy. The United States Government retains and the publisher, by accepting the article for publication, acknowledges that the United States Government retains a non-exclusive, paid-up, irrevocable, world-wide license to publish or reproduce the published form of this manuscript, or allow others to do so, for United States Government purposes. Drs. A. Y. K. Hong, T. P. Koehler, and L. J. Dechant of Sandia National Laboratories are thanked for providing insightful comments during the preparation of this paper.

REFERENCES

1. A. N. Kolmogorov, C. R. Acad. Sci. URSS 30, 301-305 (1941).
2. S. Corrsin, J. Geophys. Res. 64, 2134 (1959).
3. R. D. Moser, Phys. Fluids 18, 078105 (2006).
4. R. Betchov, J. Fluid Mech. 3, 205-216 (1957).
5. D. Bandak, N. Goldenfeld, A. A. Mailybaev, and G. Eyink, Phys. Rev. E 105, 065113 (2022).
6. R. M. McMullen, M. C. Krygier, J. R. Torczynski, and M. A. Gallis, Phys. Rev. Lett. 128, 114501 (2022).
7. J. B. Bell, A. Nonaka, A. L. Garcia, and G. Eyink, J. Fluid Mech. 929, A12 (2022).
8. P. S. Bernard, Turbulent Fluid Flow (John Wiley and Sons, Inc., Hoboken, NJ, 2019).
9. G. A. Bird, Molecular Gas Dynamics and the Direct Simulation of Gas Flows (Clarendon Press, Oxford, 1998).
10. M. Howard, A. M. Bradley, S. W. Bova, J. R. Overfelt, R. M. Wagnild, D. J. Dinzl, M. F. Hoemmen, and A. Klinvex, AIAA-2017-4407, American Institute of Aeronautics and Astronautics, Reston, VA (2017).
11. S. J. Plimpton and M. A. Gallis, "SPARTA Direct Simulation Monte Carlo (DSMC) Simulator," https://sparta.github.io/ (2022).
12. M. A. Gallis, T. P. Koehler, J. R. Torczynski, and S. J. Plimpton, Phys. Fluids 27, 084105 (2015).
13. M. A. Gallis, T. P. Koehler, J. R. Torczynski, and S. J. Plimpton, Phys. Rev. Fluids 1, 043403 (2016).
14. M. A. Gallis, N. P. Bitter, T. P. Koehler, J. R. Torczynski, S. J. Plimpton, and G. Papadakis, Phys. Rev. Lett. 118, 064501 (2017).
15. M. A. Gallis, J. R. Torczynski, N. P. Bitter, T. P. Koehler, S. J. Plimpton, and G. Papadakis, Phys. Rev. Fluids 3, 071402(R) (2018).
16. S. J. Plimpton, S. G. Moore, A. Borner, A. K. Stagg, T. P. Koehler, J. R. Torczynski, and M. A. Gallis, Phys. Fluids 31 (8), 086101 (2019).
17. M. A. Gallis, J. R. Torczynski, M. C. Krygier, N. P. Bitter, and S. J. Plimpton, Phys. Rev. Fluids 6, 013401 (2021).
18. M. A. Gallis and J. R. Torczynski, Phys. Rev. Fluids 6, 063402 (2021).
19. G. I. Taylor and A. E. Green, Proc. Royal Soc. Lon. 158 (895), 499 (1937).
20. M. E. Brachet, D. I. Meiron, S. A. Orszag, B. G. Nickel, R. H. Morf, and U. Frisch, J. Fluid Mech. 130, 411 (1983).
21. R. W. MacCormack and G. V. Candler, Comput. Fluids 17 (1), 135-150 (1989).
22. P. K. Subbareddy and G. V. Candler, J. Comput. Phys. 228 (5), 1347-1364 (2009).
23. U. Frisch, Turbulence: the legacy of A. N. Kolmogorov (Cambridge University Press, Cambridge, 1995).
24. J. Schumacher, K. R. Sreenivasan, and V. Yakhot, New J. Phys. 9, 89 (2007).
25. D. Ruelle, Phys. Lett A 72, 81-82 (1979).
26. G. Boffetta and S. Musacchio, Phys. Rev. Lett. 119, 054102 (2017).
27. A. Berera and R. D. J. G. Ho, Phys. Rev. Lett. 120, 024101 (2018).
28. N. B. Budanur and H. Kantz, arXiv 2209.01064.
29. Y. C Li, R. D. J. G. Ho, A. Berera, and Z. C. Feng, J. Fluid Mech 904, A27 (2020).
30. E. N. Lorenz, Tellus 21, 289-307 (1969).
31. A. Kupainen, Ann. Henri Poincaré 4, S713-S726 (2003).
32. G. L. Eyink and D. Bandak, Phys. Rev. Research 2, 043161 (2020).
33. S. Thalabard, J. Bec, and A. A. Mailybaev, Commun. Phys. 3, 122 (2020).
34. S. Qin and S. Liao, J. Fluid Mech. 948, A7 (2022).
35. A. Fedorov and A. Tumin, AIAA J. 55 (7), 2335 (2017).
36. P. Luchini, AIAA J. 55 (1), 121 (2017).